Geoderma 467 (2026) 117712

Contents lists available at ScienceDirect

Geoderma

journal homepage: www.elsevier.com/locate/geoderma

Spectroscopic analysis shows crandallite can be a major component of soil phosphorus

Christian Vogel [a,*,1], Julian Helfenstein [b,c,1], Michael Massey [d,e], Ruben Kretzschmar [f], Ulrich Schade [g], René Verel [h], Oliver Chadwick [i], Emmanuel Frossard [b]

[a] Bundesanstalt für Materialforschung und –prüfung (BAM), Unter den Eichen 87, 12205 Berlin, Germany
[b] Institute of Agricultural Sciences, ETH Zurich, 8315 Lindau, Switzerland
[c] Soil Geography and Landscape Group, Wageningen University & Research, 6700 Wageningen, the Netherlands
[d] Department of Earth and Environmental Sciences, California State University East Bay, Hayward, CA 94542, USA
[e] Present address: Environment Canterbury, Christchurch 8140, New Zealand
[f] Institute of Biogeochemistry and Pollutant Dynamics, CHN, ETH Zurich, 8092 Zurich, Switzerland
[g] Helmholtz-Zentrum Berlin für Materialien und Energie GmbH, Hahn-Meitner-Platz 1, 14109 Berlin, Germany
[h] Department of Chemistry and Applied Biosciences, ETH Zurich, 8093 Zurich, Switzerland
[i] Department of Geography, University of California, Santa Barbara, CA 93106, USA

ARTICLE INFO

Handling Editor: Dr. Andrew Margenot

Keywords:
Phosphorus transformations
Soil development
powder X-ray diffraction
P K-edge X-ray absorption spectroscopy
micro-infrared spectroscopy
solid-state ^{31}P nuclear magnetic resonance (NMR) spectroscopy

ABSTRACT

Phosphorus (P) bioavailability is crucial for the productivity of natural and agricultural ecosystems, and soil P speciation plays a major role therein. Better understanding of P forms present in soil is thus essential to predict bioavailability. However, P speciation studies are only as powerful as the reference spectra used to interpret them, and most studies rely on a limited set of reference spectra. Most studies on soil P forms differentiate between Ca-bound P (e.g. apatite), organic P, Fe-bound P, and Al-bound P. In our analysis of a Ca, Al, and P rich soil from the Kohala region of Hawaii, we identified the mineral crandallite, $CaAl_3(PO_4)_2(OH)_5{\cdot}H_2O$, a mineral previously not considered to play a significant role in soils. Crandallite was first identified with powder X-ray diffraction. Subsequently reference spectra were collected, and the presence of crandallite was confirmed using micro-focused P *K*-edge X-ray absorption near edge structure (XANES) spectroscopy, micro-infrared spectroscopy, and solid-state ^{31}P nuclear magnetic resonance (NMR) spectroscopy. Crandallite XANES spectra were distinct from other common XANES spectra due to the presence of features in the post-edge region of the spectrum. Linear combination fitting of bulk P *K*-edge XANES spectra allowed the determination of the proportion of crandallite to the total P content, indicating that crandallite comprises up to half, possibly even more of the soil P in the samples. Crandallite is therefore an important and potentially overlooked component of soil P, which pedogenically forms in soils with high P, Al, and Ca contents, where it could play an important role in P bioavailability.

1. Introduction

Phosphorus (P) is an essential plant nutrient, and as such its bioavailability directly affects ecosystem functions relevant for crop yields, water quality, and carbon sequestration (Helfenstein et al., 2024). Soil phosphorus undergoes numerous transformations that impact its bioavailability, including dissolution/precipitation, adsorption/desorption, biological uptake, and mineralization of organic P (Frossard et al., 2000; Helfenstein et al., 2024). The magnitude of these fluxes between geochemical and organic pools depends largely on the P forms present in the soil.

Phosphorus forms in soils are commonly classified into organic P, calcium-bound P (Ca-P), iron-bound P (Fe-P), and aluminum-bound P (Al-P). Walker and Syers (1976) described a pedogenic trend in which the dominant P forms shift from apatite (Ca-P) in young soils to organic P and Fe- or Al-associated P—either adsorbed or occluded—in highly weathered soils. Although it has been recognized since at least the 1980s that soils and sediments contain a wide array of specific P species

* Corresponding author.
E-mail address: christian.vogel@bam.de (C. Vogel).
[1] Shared first-authorship.

https://doi.org/10.1016/j.geoderma.2026.117712
Received 1 October 2025; Received in revised form 18 November 2025; Accepted 31 January 2026
Available online 11 February 2026

(Nriagu, 1984), the majority of studies continue to broadly categorize soil P into apatite, organic P, Fe-bound P, and Al-bound P. For instance, the widely used Hedley sequential fractionation method (Hedley et al., 1982) is still commonly interpreted such that NaOH-extractable P represents Fe- and Al-associated forms, and HCl-extractable P corresponds to apatite and other Ca-associated forms, despite increasing criticism of these assumptions (Gu and Margenot, 2021; Klotzbücher et al., 2019). Likewise, synchrotron-based P speciation techniques frequently group inorganic soil P into Ca-, Al-, and Fe-associated forms (Eriksson et al., 2016; Koch et al., 2018; Prietzel et al., 2013).

Our previous analysis of soils from the Kohala climosequence in Hawaii, X-ray diffraction (XRD) revealed the presence of crandallite, a Ca-Al-phosphate with the chemical formula $CaAl_3(PO_4)_2(OH)_5{\cdot}H_2O$, in several soils (Vogel et al., 2021). Crandallite is not commonly considered a relevant soil P species, and this finding challenged the paradigm that inorganic soil P can be split into Ca, Al or Fe associated P, since P in crandallite is associated with both Ca and Al. While crandallite has been documented in environmental samples using earlier methods such as XRD and ^{31}P solid-state nuclear magnetic resonance (NMR) spectroscopy (Adams et al., 1973; Bleam et al., 1989; Frossard et al., 1995; Young et al., 2019), these methods are not frequently used to study P speciation in soils due to relatively low detection and quantification limits and poor spectral resolution (Kruse et al., 2015). Still, crandallite has been detected in soils developed on coral atolls (Borggaard et al., 2012; Fieldes et al., 1960) and in places receiving long-term (centuries to millennia) application of animal bones, wastes, and plant residues (Costa et al., 2004; Frost et al., 2011; Goldberg and Nathan, 1975). Investigators such as Garrett et al. (2010) and Batista et al. (2017) inferred the presence of crandallite in soil samples based on visual examination with scanning electron microscopy, along with elemental ratios from energy dispersive spectroscopy (SEM-EDS). Newer, more sensitive techniques such as infrared (IR) or X-ray absorption near-edge structure (XANES) spectroscopy have not reported crandallite, likely because no reference spectra have been available (Prietzel et al., 2016; Vogel et al., 2016). Though XRD and ^{31}P solid-state NMR spectroscopy can be used to identify the presence of crandallite in soils with exceptionally high crandallite content, the availability of reference spectra for micro-spectroscopic techniques would open the door to identification of crandallite in other soils.

The objectives of the present work were to 1) measure reference spectra for crandallite for multiple P speciation methods, 2) apply additional P speciation techniques in order to consolidate whether the presence of crandallite could be confirmed in the Hawaiian samples, and 3) to quantify the contribution of crandallite to soil P. We selected three methods to complement the X-ray diffraction: P *K*-edge XANES spectroscopy, micro-Fourier transform infrared spectroscopy (micro-FT-IR) spectroscopy, and solid state ^{31}P NMR. Our hypotheses were that measuring reference spectra of crandallite with these methods would allow identification of crandallite in the soil samples, supporting the results reported in Vogel et al. (2021). Furthermore, we hypothesized that crandallite constitutes a major soil P form in these tropical soils developed on alkalic basalt. In the discussion we discuss agronomic and environmental implications of crandallite.

2. Materials and methods

2.1. Crandallite acquisition, sampling, and characterization

A mixed mineral of crandallite, variscite, and wardite was acquired from a commercial source. The specimen was from the Little Green Monster claim in Clay Canyon, Fairfield, Utah, United States of America. The mixed specimen was composed of relatively large portions of each mineral, whereby the crandallite minerals had the characteristic light yellow color (Nriagu, 1984), surrounding the green variscite. Our analyses also found apatite and quartz in the specimen, which were not mentioned in the commercial description likely because they were minor components. As the bulk sample was a heterogeneous assemblage of different minerals, a small portion that appeared rich in thin layers of yellow crandallite was broken off the bulk sample and subsampled to obtain a powdered sample of comparatively homogeneous (but not pure) crandallite. Pieces of light yellow crandallite of this specimen were separated by visual assessment, followed by careful hand-picking of crandallite fragments. Larger fragments were used for micro-focused X-ray analysis. A small quantity (~30 mg) of crandallite was selected and powdered for XRD, FT-IR spectroscopy, and bulk P *K*-edge XANES spectroscopic analyses.

2.2. Soil sampling

Samples of A and B horizons were taken from two soils on 150,000 years Hawi lava flows on Kohala Volcano, Hawaii. The soils were sampled as part of a larger study designed to understand the influence of climate on the sources and transformations of P in volcanic soils (Helfenstein et al., 2018; Vogel et al., 2021). Here Site 1 is the same as Site 4 and Site 2 is the same as Site 3 in those previous papers. The two sites straddle the udic – ustic moisture regime transition with Site 1 receiving 1578 mm of mean annual precipitation (MAP) and Site 2 receiving 1340 mm of MAP (Giambelluca et al., 2013). Each site is subject to wet – dry cycles annually (Hsieh et al., 1998). Site 1 was sampled in the Palapalai Soil Series (Hydrous, ferrihydritic, isothermic Eutric Hydrudands) and Site 2 was sampled in the Waimea Soil Series (Medial, amorphic, isothermic Humic Haplustands). The A horizon sampling depths were 30 (Ap1 and Ap2 horizons combined) for Site 1 and 15 cm (A1 and A2 horizons combined) for Site 2 with the thicker A horizons in the Palapalai soil reflecting more positive water balance (MAP-Potential Evapotranspiration; Table S1) compared with the drier Waimea soil. The B horizon sampling depths were 30–50 cm and 15–40 cm, for Sites 1 and 2 respectively. Further details on sampling protocols can be found in Helfenstein et al. (2018). The soils are strongly weathered, but retain a substantial supply of nutrients (non-hydrolyzing cations and phosphorus) (Bullen and Chadwick, 2016; Chadwick et al., 2007; Vitousek and Chadwick, 2013) and lie in the kinetically-limited soil process domain as described by Chadwick et al. (2022). Hawi lava flows have alkalic chemistry with relatively high levels of total P which is inherited by the soil profiles (Bullen and Chadwick, 2016; Spengler and Garcia, 1988). Site and soil chemical data are summarized in Table S1 and S2. Crandallite was first identified in these soils using XRD (Vogel et al., 2021). Here we conduct a detailed analysis of Crandallite in the < 2-mm fraction of the sampled horizons using XRD, micro-focused FT-IR spectroscopy, bulk XANES, micro-focused XRF in combination with micro-XANES and solid-state ^{31}P NMR spectroscopy. P cycling in these soils has been described in previous studies (Helfenstein et al., 2021; Helfenstein et al., 2018; Siegenthaler et al., 2020; Vogel et al., 2021). In brief, both chemical extraction and isotope exchange kinetic experiments confirmed that these soils have extremely high amounts of available P due to high total P levels from the basaltic parent material, and most P is in adsorbed forms with varying turnover rates (Helfenstein et al., 2018). The high P values are explained by a combination of high inputs and low P losses. The main input is from rock weathering, and these nutrients accumulate in the topsoil through the process of biological uplift, with dust input playing a secondary role (Vitousek and Chadwick, 2013). Losses are minimal at this site because constant soil cover limits erosion and high sorption capacity and only moderate levels of rainfall limit P leaching (Helfenstein et al., 2018).

2.3. Powder X-ray diffraction and Rietveld analysis

X-ray diffractograms from the Little Green Monster crandallite powder were collected using a Rigaku MiniFlex 600 in transmission geometry, using a Cu Kα X-ray source and a D/teX 0D strip detector. For the Kohala soils, XRD patterns were collected using a Bruker D8 Advance diffractometer using Cu $K\alpha_{1,2}$ radiation and a high-resolution energy-

dispersive 1D detector (Bruker AXS GmbH, Karlsruhe, Germany). The data were collected in Bragg-Brentano geometry from 4° to 70° 2θ with 0.02° 2θ steps and 10 sec acquisition time per step. For the determination of "amorphous" matter contents, X-ray diffractograms were also collected after mixing powdered samples with 33% w/w crystalline corundum powder (Al_2O_3) as an internal standard. The diffractograms were analyzed with Rietveld quantitative-phase analysis using TOPAS Version 5 (Bruker DIFFRAC.SUITE). While XRD was already applied to the soil samples in the Vogel et al. (2021) study, these results are presented in more detail here, together with diffractograms and spectra of the reference crandallite sample.

2.4. Micro-focused FT-IR spectroscopy

Synchrotron IR chemical mapping was performed with a Thermo Continuμm IR microscope coupled to a Thermo Nicolet Nexus 870 spectrometer at the IRIS beamline of the synchrotron BESSYII, Berlin, Germany (Energie, 2016). The soil samples were mapped in transmission mode after compression between two diamond windows (Vogel et al., 2013). An aperture of 10 × 10 μm^2 and a step size of 10 μm were used for mapping (spectral resolution 8 cm^{-1}; 128 scans were co-added per spectrum).

2.5. Bulk X-ray absorption near edge structure (XANES) analysis

In order to obtain X-ray spectroscopic estimates of P speciation, bulk P *K*-edge XANES spectra of crandallite and soils were collected on Beamline 14–3 at the Stanford Synchrotron Radiation Lightsource (SSRL) at SLAC National Accelerator Laboratory in Menlo Park, California. Crandallite was diluted 20:1 with confectioner's sugar prior to analysis, and all samples were ground and homogenized by hand using an agate mortar and pestle. A small quantity of powder from each finely ground, homogenized sample was painted on ultra-low impurity carbon tape (Ted Pella, Inc.) using a synthetic-bristle paintbrush to avoid P contamination. Incident beam energy was selected using a Si(111) double crystal monochromator in the phi = 90° position, and the beam path was continuously purged with helium. Energy calibration was achieved by setting the top of the primary *K*-edge peak of the lazulite XANES spectrum to 2153.5 eV.

After data collection, multiple spectra were averaged using the Six-Pack software package (Webb, 2005). Data normalization and analysis of the bulk P *K*-edge XANES spectra were conducted using Athena (Ravel and Newville, 2005). Linear combination fitting of the normalized P *K*-edge XANES spectra was performed to quantify P speciation in the materials. Standard spectra used for linear combination fitting included crandallite (collected in this study), and an Al oxide-humic P complex (Giguet-Covex et al., 2013). P *K*-edge XANES fits used the least number of reference spectra required to describe the data (usually 1–2 reference spectra), and reference spectra that did not significantly contribute to the fits were not included in the final analysis.

2.6. Micro-focused X-ray fluorescence and micro-XANES analysis

Micro-focused X-ray fluorescence mapping (micro-XRF) and micro-focused P *K*-edge XANES (micro-XANES) were also carried out at SSRL Beamline 14–3. Sample preparation, data collection, and data analysis for micro-XRF and P micro-XANES were similar to the procedures described in Massey (2019). Samples were encased in optical epoxy (Epotek 301-2FL), cut to expose soil grains, and lightly polished prior to analysis. Micro-XRF maps were analyzed using the SMAK software package, and micro-XANES spectra were analyzed in a manner similar to the bulk XANES analysis, described above.

2.7. Solid state MAS ^{31}P NMR spectroscopy

Solid-state 31P DPMAS-NMR spectra of Site 1A and additionally of the A horizons of a arid (275 mm rainfall) and a humid site (3123 mm rainfall) from the Kohala site were recorded on a Bruker AvanceIIIHD 500 spectrometer equipped with a 11.75 Tesla Magnet and operating at a 31P Larmor frequency of 202.5 MHz. The samples were measured using a Magic Angle Spinning Double Resonance Probehead and were packed in 2.5 mm o.d. rotors. The rate of rotation was 24 kHz. The ^{31}P chemical shift scale is referenced to H_3PO_4 (85%) using the ^{31}P signal of $(NH_4)H_2PO_4$ at 2.5 ppm as a secondary reference. Spectra were acquired with a pulse width of 1.4 μ s (corresponding to a pulse flip angle of 45°), an acquisition time of 0.00328 s, a spectral width of 1543 ppm, a recycle delay of 0.7 s and 16,384 scans. The P species observed in the spectra were derived from the isotropic chemical shift values provided by Young et al. (2019) for reference minerals.

3. Results

3.1. XRD analysis of crandallite and Kohala soil

Rietveld analysis of XRD patterns revealed that the powdered sample of the yellow crandallite part of the Little Green Monster that was used to obtain the bulk P *K*-edge XANES and FT-IR reference spectra contained ~ 78% crandallite and ~ 22% quartz, with the possibility of additional minor trace constituents. Rietveld analysis of XRD patterns from the Kohala soils also found crandallite in the A and B horizon, in addition to major minerals such as quartz (see also Vogel et al. (2021)). XRD patterns and Rietveld fits are depicted in Fig. 1.

3.2. Micro-focused FT-IR spectroscopic investigation of Kohala soil

Two out of 736 micro-FT-IR spectra from the A horizon of site 2 soil showed absorption bands that are very similar to that of the Little Green Monster crandallite reference (Fig. 2). The intense bands at 1034 cm^{-1} (arrow 1) and 1099 cm^{-1} (arrow 2) are assigned to the symmetric stretching modes of the PO_4^{3-} units (Breitinger et al., 2006; Frost et al., 2011). The IR bands at 1066, 1109, 1140 and 1182 cm^{-1} are assigned to the antisymmetric stretching modes of the PO_4^{3-} and HPO_4^{2-} units (Frost et al., 2011; Grey et al., 2011). Moreover, there are several other spectra that are close to crandallite but have a slightly shifted bands that are probably mixed mineral with other Al-phosphates. Furthermore, for aluminum phosphates the τ(P–O) and $\nu(O_3P–O)$ bands between 900–700 cm^{-1} are characteristic for their mineral form and can also distinguish between the berlinite, phosphotridymite and cristobalite forms (Farmer, 1974). For our sample these IR bands are at 780 and 802 cm^{-1} (arrow 3), which comes very close to our reference (779 and 799 cm^{-1}). However, in the literature there is not a clear assignment for these bands (Breitinger et al., 2006; Frost et al., 2011).

3.3. Phosphorus K-edge XANES and micro-XRF map of Little Green Monster crandallite

Micro-XRF mapping (Fig. 3, top) and P *K*-edge micro-XANES (Fig. 3, bottom) of the Little Green Monster reference specimen revealed a dominant P form with a previously undescribed spectra, which we assumed to be crandallite, as well as some mineralogical heterogeneity. The micro-XANES spectrum of wardite was similar to previously published spectra (Ingall et al., 2011).

The bulk and micro-focused P *K*-edge XANES spectra of crandallite (Fig. 3 bottom) had a relatively narrow whiteline at ~ 2153.3 eV, with a peak position and shape similar to that of P adsorbed to Al oxides. The primary peak lacked the characteristic "shoulder" feature associated with XANES spectra from other Ca-phosphates, and also did not exhibit peak broadening in a manner similar to P adsorbed on calcite (Giguet-Covex et al., 2013). The spectrum was also distinct from other Al-phosphates, however, in that it exhibited a post-edge bump that extended to about 2162.5 eV. After the bump a unique and distinct "valley" (local minimum) feature occurred, centered at ~ 2165 eV. As a

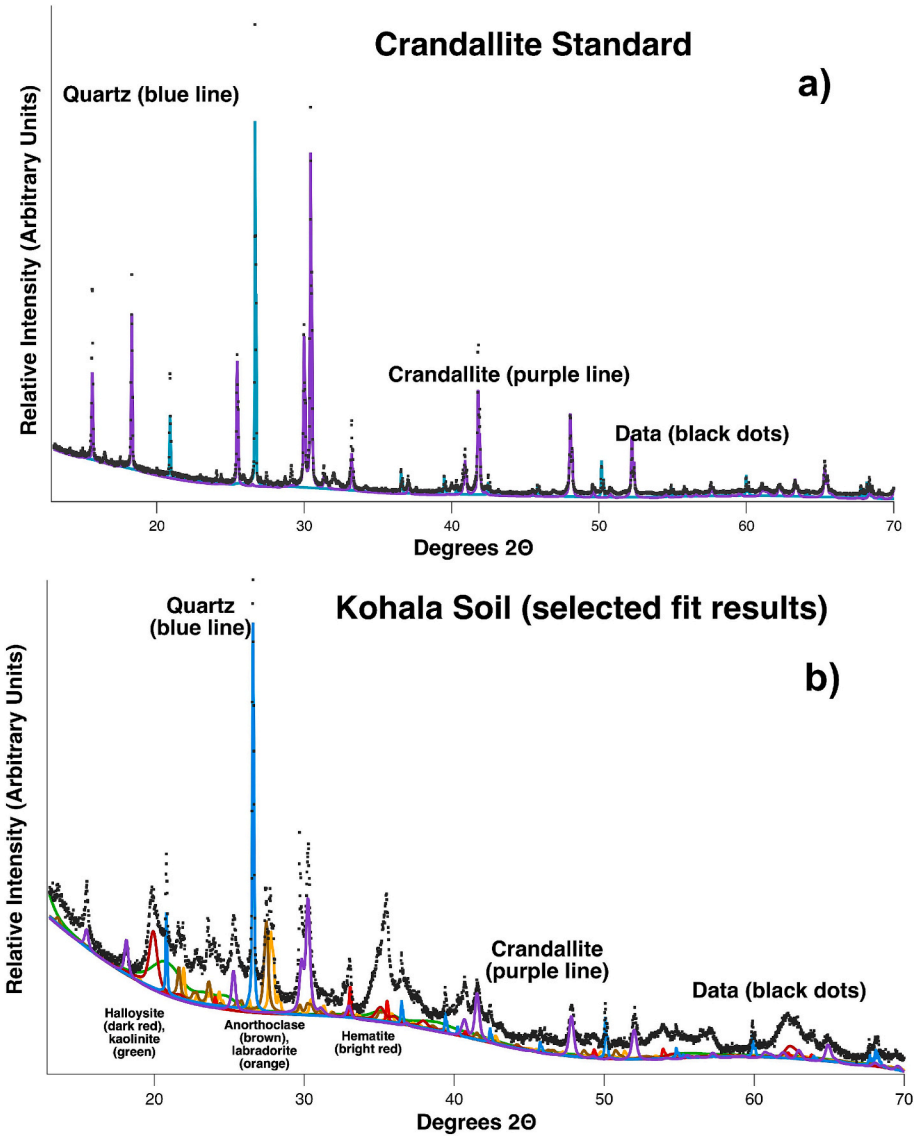

Fig. 1. X-ray diffractograms and simplified, partial Rietveld fitting results from a) the yellow crandallite part of the Little Green Monster (78% crandallite, 22% quartz), and b) the Kohala 2A soil. Data are shown as dots, while fits are shown as lines (blue = quartz, purple = crandallite, bright red = hematite, dark red = halloysite, brown = anorthoclase), and the fit residual is shown underneath each diffraction pattern.

result of these post-edge features, the diffuse post-edge "mound-shaped" peak typically found in most P *K*-edge XANES spectra was considerably narrower and sharper in the crandallite spectra. The combination of these post-edge features distinguished the crandallite P *K*-edge XANES spectra from that of other Ca- and Al-phosphate species.

3.4. Phosphorus K-edge XANES and micro-XRF map of Kohala soil

Micro-XRF mapping (Fig. 4 left) and P *K*-edge micro-XANES (Fig. 4 right) showed considerable heterogeneity in the speciation of P in the Kohala soil 2A at the micro-scale. Crandallite was found at the micro-scale, as were spectra with the characteristic apatite-like post-edge "shoulder," spectra with a pre-edge feature indicating Fe-associated P (e.g., Beauchemin et al. (2003)), and relatively featureless spectra indicating Al-associated P (Fig. 4, right).

Linear combination fitting of bulk P *K*-edge XANES spectra of both soils (Fig. 5a) indicated that crandallite accounts for 41–57% of total P in three of the four studied Kohala soils (Table 1).

The bulk spectrum from the A horizon of Site 1 could be fit with only one component, an Al-humic P complex, but the fit of the spectrum from the B horizon of Site 1 suggested ~ 43% of total P was crandallite. Visual inspection of the spectrum and fit (Fig. 5a) left open the possibility that the crandallite contribution to the spectrum was over-estimated, due to the absence of the characteristic post-edge "shelf" and "valley" features. However, the broad post-edge "mound" feature is perhaps slightly sharper in the B horizon spectrum from Site 1. Note that the total uncertainty in the fits is approximately ± 15%, as discussed extensively elsewhere (e.g., Massey et al. (2018), Massey (2019)).

The linear combination fits of spectra from Site 2 were considerably less ambiguous: crandallite was ~ 57% of total P in the A horizon of Site 2, and ~ 41% of total P in the B horizon of the same site. The post-edge features were associated with crandallite and clearly visible in both bulk spectra from Site 2, suggesting that crandallite did indeed contribute significantly to the bulk spectrum of this soil. For comparison, other common spectra such as apatite P, Al- and Fe-associated adsorbed P, and organic matter P are shown in Fig. 5b, and generally bear little resemblance to the bulk spectra from these Kohala soils. Despite the micro-scale heterogeneity depicted in Fig. 4, crandallite appeared to be a major portion of soil P, at least at Site 2, and potentially in the B horizon of Site 1.

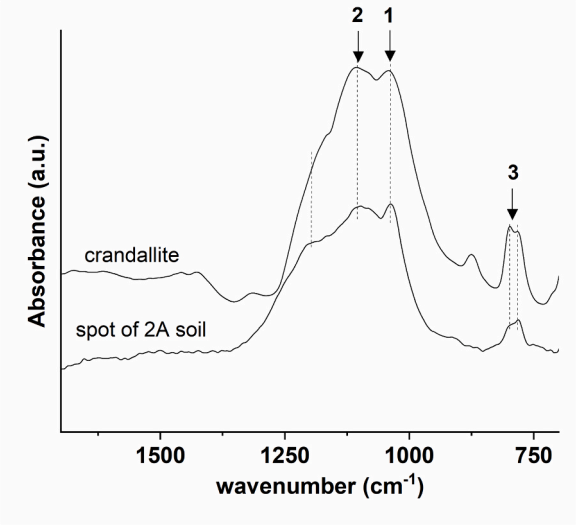

Fig. 2. Comparison of micro-FT-IR spectrum of soil from site 2A (bottom) and crandallite standard (isolated crandallite from Little Green Monster, top). The bands arrow 1 and arrow 2 are assigned to the symmetric stretching modes of the PO_4^{3-} units. Arrow 3 are the aluminum phosphates the τ(P–O) and ν(O_3P–O) bands.

3.5. Solid-state ^{31}P NMR spectroscopy

Fig. 6 shows the solid-state ^{31}P NMR spectra of the sub-humid Site 1A as well as the arid and humid sites of the Hawi flow, respectively. The position of the major ^{31}P NMR signal of sample 1A (Fig. 6 top) refers to crandallite (see arrow 2 at approx. −5.2 ppm; (Bleam et al., 1989)), but the sample also contains some apatite, as seen by the small peak at approx. 4 ppm (arrow 1). The apatite signal of site 1A is also in agreement to the apatite signal of the arid site of the Kohala climosequence (Fig. 6 middle), where apatite is the dominant soil P species (Helfenstein et al., 2018). The shoulder located at the right of the main apatite peak in this arid site also suggests the presence of crandallite as a secondary P mineral. The humid site (Fig. 6 bottom) on the other hand shows only minimal or no apatite signal, but a broad signal which mostly is a combination of crandallite (arrow 2) and wavellite (arrow 3; −11.2 ppm). The width of the mean peak at half height might also suggest differences in P mineral crystallinity with apatite at the drier site having a high level of crystallinity, while the P forms found in the other sites being less well organized.

4. Discussion

Collection of reference spectra for crandallite and application of four spectroscopic techniques confirmed the presence of crandallite in the soil samples from the Hawi lava flow on the Kohala climatic gradient on Hawaii. Furthermore, crandallite was determined to be a dominant soil P form in three out of four of the samples, constituting around half of total soil P. Below, we discuss the environmental and agronomic implications, namely how the identification of crandallite in the studied soils relates to the geochemical and ecological processes described at this site. This enables conclusions to be drawn about the conditions under which crandallite might be expected to play an important role in soil P cycling in other soils around the world. Second, we discuss the methodological considerations arising from this work and implications for future studies.

4.1. Environmental and agronomic implications

Crandallite forms according to the following reaction:

$$Ca(OH)_{2(s)} + 2\,AlPO_4{\cdot}2H_2O_{(s)} + Al(OH)_{3(s)} \rightarrow CaAl_3(PO_4)_2(OH)_5{\cdot}H_2O_{(s)} + 3\,H_2O_{(l)}.$$

Hence, high Ca, Al, and P availability are necessary to precipitate crandallite (Nriagu, 1976). Several observations on soil properties and processes from previous work on the studied soils support the hypothesis that crandallite is formed in-situ in these soils. In the studied soils developed on alkaline basalt in a tropical climate, Al concentrations extractable with pyrophosphate, oxalate ammonium, or dithionite-citrate-bicarbonate are all > 10 g kg^{-1}, indicating high presence of Al-oxides in various amorphous to crystalline phases (Helfenstein et al., 2021). Similarly, total Ca (> 5000 mg kg-1) and P (> 2000 mg kg-1) concentrations are very high in these soils (Vitousek and Chadwick, 2013). The exceptionally high Ca and P concentrations have been explained by the weathering of apatite in the subsoil and subsequent "pumping" and accumulation of Ca and P into upper soil horizons by biological uplift (Bullen and Chadwick, 2016; Helfenstein et al., 2018; Porder and Chadwick, 2009; Vitousek and Chadwick, 2013). Rainfall drives weathering, the loss of base cations such as Ca, and a subsequent decline in pH on the subhumid site (Vitousek and Chadwick, 2013). The drop in pH might then lead to increased dissolution of apatite (Ca-P) in the subsoil, as well as the deepening of the weathering front in the parent material, exposing more apatite from parent material for dissolution (Chadwick et al., 2003). The documented translocation of released Ca and P ions by plants from the subsurface to the topsoil (the "biological nutrient pump") leads to the accumulation of increased amounts of exchangeable P and Ca in surface soil horizons (Bullen and Chadwick, 2016; Helfenstein et al., 2018; Porder and Chadwick, 2009; Vitousek and Chadwick, 2013). These processes thus create an environment that we interpret to be conducive to crandallite precipitation.

The detection of crandallite also helps to further our understanding of pedogenesis and P biogeochemistry in these soils. Crandallite, due to its low solubility, could accumulate in the soil and protect Ca and P from losses via leaching at intermediate weathering stages where pH starts to decline (unfavorable for apatite) but some Ca continues to remain in the soil profile. This could explain why we find crandallite at subhumid sites, corresponding to intermediate weathering stages, and which had pH in the range of 5.9 and 6.6 (Vogel et al., 2021), but not at the arid sites. At acidic pH, crandallite is only considered to be *meta*-stable (Nriagu, 1976), despite being detected in soils with a pH as low as pH 5 (Fischer et al., 2018). Thus, in these sites, crandallite might precipitate and re-dissolve readily, explaining the high P exchange fluxes measured (Helfenstein et al. 2018). With further weathering, as is the case for the humid sites along the climate gradient, leaching losses of Ca and further drop in pH create unfavorable conditions for crandallite conditions, explaining why no crandallite is found at wetter sites.

Notably, detection of crandallite now enables more robust interpretation of sequential extractions and isotope incorporation across these pools, clarifying results that had remained unresolved in earlier studies (Helfenstein et al., 2021; Helfenstein et al., 2018). Stable oxygen isotopic signature of phosphate on the subhumid Kohala sites revealed that both the sodium hydroxide-extractable inorganic P (NaOH-Pi) and the hydrochloric acid-extractable inorganic P (HCl-Pi) pools were in equilibrium with the stable oxygen isotope composition of resin-P (Helfenstein et al., 2018), indicating significant exchange between these pools of inorganic P. In addition, tracing of P exchange in these Hawaiian soils with radioisotopic methods showed that the majority of P was cycling in a timescales of weeks to months, suggesting dominance of adsorbed and or *meta*-stable P precipitates (Siegenthaler et al., 2020). However, 25–33% of added radioisotope was not recovered in the Hedley sequential extraction (Helfenstein et al., 2021). Sequential extraction of crandallite has shown that crandallite P is partially extractable by HCl and partially by NaOH, with a large amount remaining as residual P (Williams et al., 1980). This explains our previous observation that in the Hawaiian soils NaOH and HCl extractable P had surprisingly similar dynamics in terms of tracer uptake and exchange, and a large part of the radioisotopic tracer was not recoverable, since it was likely in residual crandallite P precipitates.

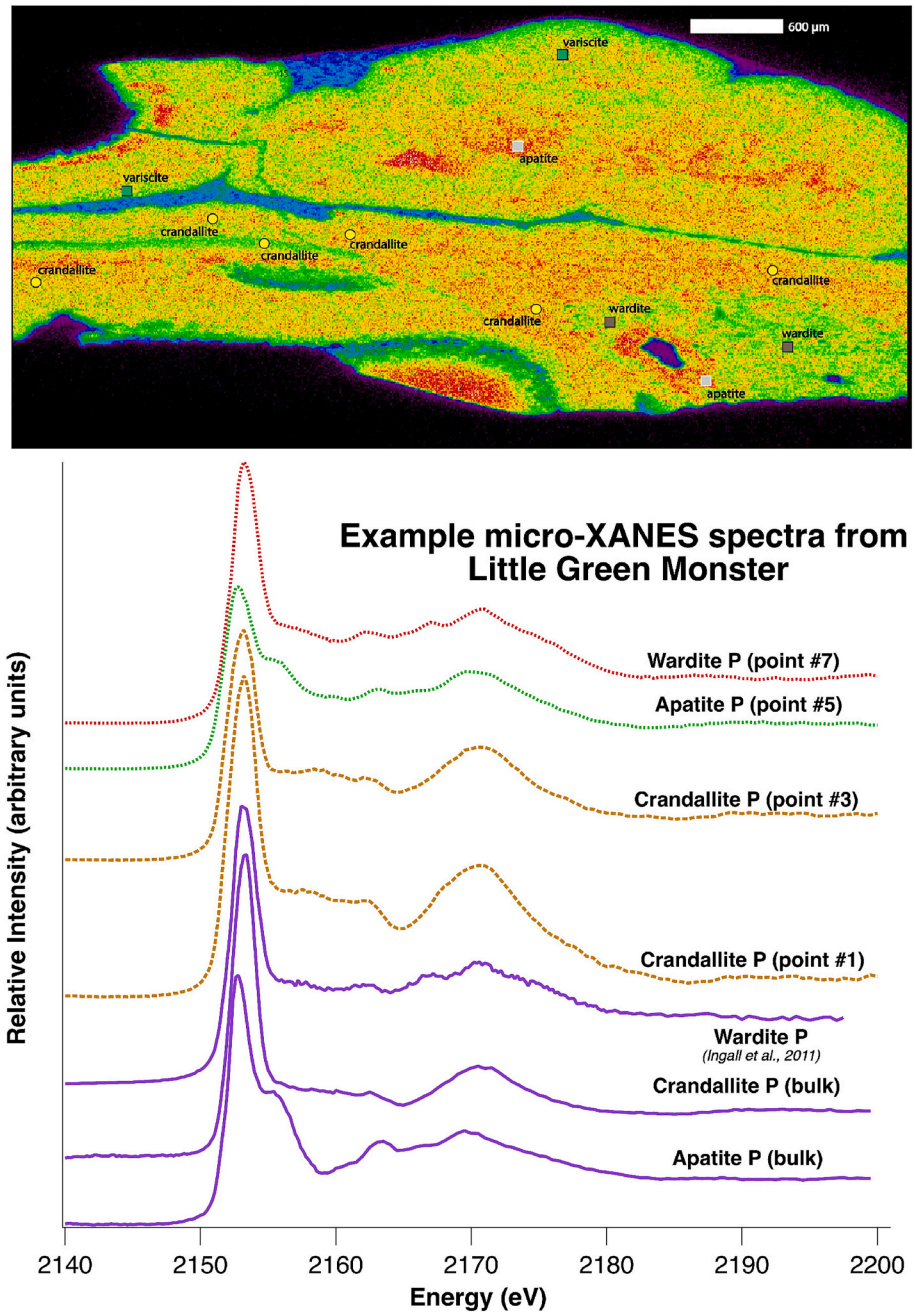

Fig. 3. Micro-focused X-ray spectroscopic analyses of a larger fragment consisting of crandallite, wardite, and apatite from the Little Green Monster claim. Micro-XRF map showing P fluorescence (red = high concentration, blue = low concentration) and micro-XANES spectroscopy analysis points (top) speciated with XANES linear combination fitting; selected micro-focused and bulk P K-edge XANES spectra of apatite, wardite and crandallite (bottom).

The possible favorable nutrient availability from crandallite was previously discussed in the literature, as crandallite from coral atolls and Brazilian phosphate deposits were applied as fertilizer on agricultural land (Bolland and Allen, 1987; Bolland and Gilkes, 1990; Doak et al., 1965; Francisco et al., 2008). Furthermore, earlier studies had documented crandallite in heavily fertilized sites, such as areas receiving household waste (Costa et al., 2004; Fischer et al., 2018; Frost et al., 2011; Goldberg and Nathan, 1975). While Goldberg and Nathan (1975) identified crandallite with XRD, Frost et al. (2011) used XRD and Raman spectroscopy, and Fischer et al. (2018) FT-IR spectroscopy. We speculate that practices of liming and P fertilizer application, which are widespread in agricultural soils, could also create conditions favorable to crandallite formation. For example, it has been reported that crandallite forms in Brazilian Oxisols after P fertilizer application, binding P and reducing risk of P losses (Fischer et al., 2018). This would imply that crandallite might be an overlooked P form in agricultural soils worldwide, especially in areas with high Al, P, and Ca availability and soil pH in the range of circa pH 5 to pH 6.5.

4.2. *Methodological considerations*

Soil P species have been analyzed with a broad set of methods, e.g. XRD, NMR, XANES, infrared and Raman spectroscopy (Helfenstein et al., 2024; Kruse et al., 2015; Vogel et al., 2016). On the subhumid sites of the Hawi lava flow on the Kohala volcano, four independent spectroscopic analytical techniques found crandallite to be a predominant or co-dominant form of soil P despite substantial microscale heterogeneity.

To analyze soil transformation processes, X-ray crystallographic

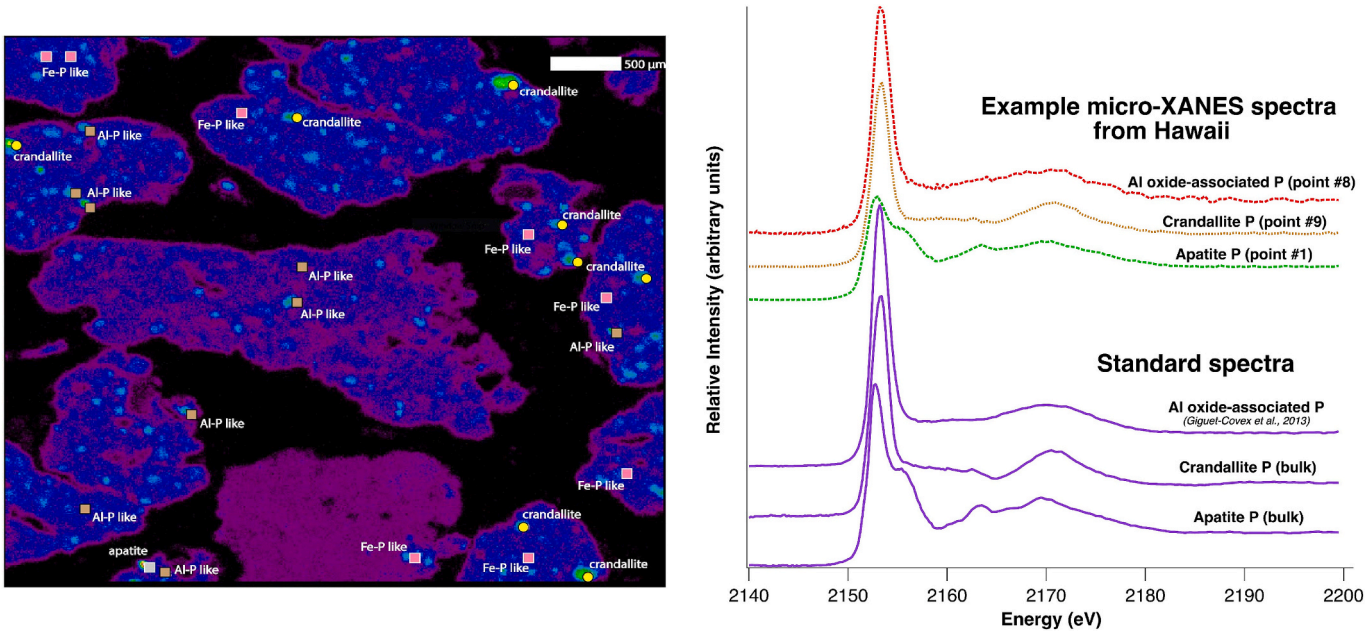

Fig. 4. Micro-focused X-ray spectroscopic analyses of the 2A soil from Kohala, Hawaii: Micro-XRF map showing P fluorescence (green = high concentration, purple = low concentration) and micro-XANES spectroscopy analysis points (left) speciated with XANES linear combination fitting; selected micro-focused and bulk P K-edge XANES spectra of crandallite, apatite, and adsorbed P species (right).

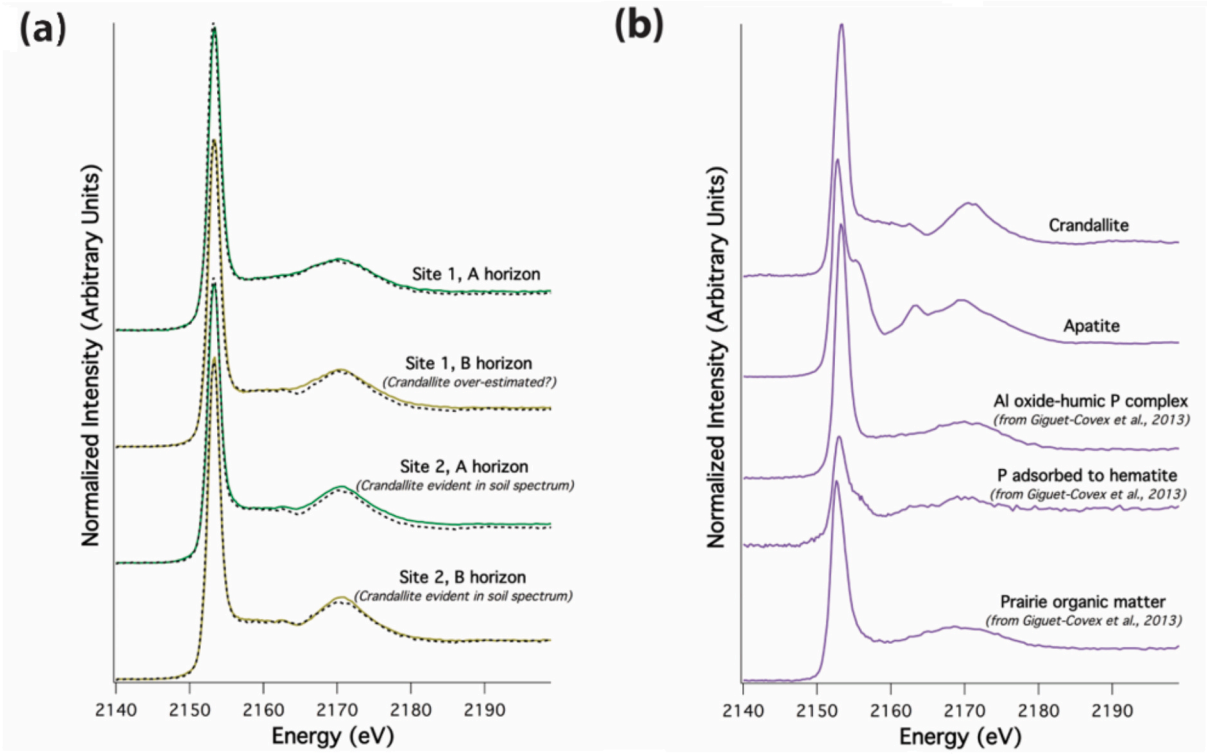

Fig. 5. Bulk P K-edge XANES spectra: (a) XANES spectra (solid lines) and linear combination fits (dashed lines) from the A and B horizons of Kohala soils at two different sites; (b) XANES spectra of known materials, including crandallite, apatite, and several types of adsorbed and organic P.

methods such as XRD have long been used to interrogate soil mineralogy, but generally only crystalline solids are "visible" in powder X-ray diffractograms (Kizewski et al., 2011). Additionally, minor mineral constituents might not be identifiable via XRD, though they can be found by other methods such as electron microscopy (Batista et al., 2017). According to XRD analytical results, 0.7% and 4.9% of the dry mass in A horizon of site 1 and 2 (Vogel et al., 2021) from the Hawi soils, respectively, was crandallite. By comparing this to total P concentrations as determined by XRF (see Table S2), we calculate that 17% and 41% of soil P was in the form of crandallite. The same approach yields 44% and 49% P as crandallite in the B horizons of the same sites.

^{31}P solid-state nuclear magnetic resonance (NMR) spectroscopy was previously applied to directly analyze soil P; however, applications of this technique are limited due to the low concentration of P in most soils

Table 1
Bulk phosphorus K-edge XANES linear combination fitting results for the two Kohala soils from the subhumid sites (Fig. 5a). Sums of components in the linear combination fits were normalized to 100%. R-factor, X^2, and reduced X^2 values were calculated by the Athena software package. Uncertainty, in parentheses, is statistical uncertainty calculated by Athena; total uncertainty was approximately ± 15%.

	Soil Horizon	Al-humic. P	Crandallite P	*R*-factor	X^2	Red. X^2
		—— P % ——				
Site 1	A	100% (†)		0.009118	3.32637	0.022176
	B	57% (±6%)	43% (±8%)‡	0.009145	3.43036	0.022869
Site 2	A	43% (±4%)	57% (±5%)	0.006110	1.90703	0.012629
	B	59% (±3%)	41% (±4%)	0.002702	1.07684	0.007131

† Uncertainty in cases where the fit required only one component are approximately equal to the total uncertainty.
‡ The fit suggests that this result overestimates the contribution from crandallite.

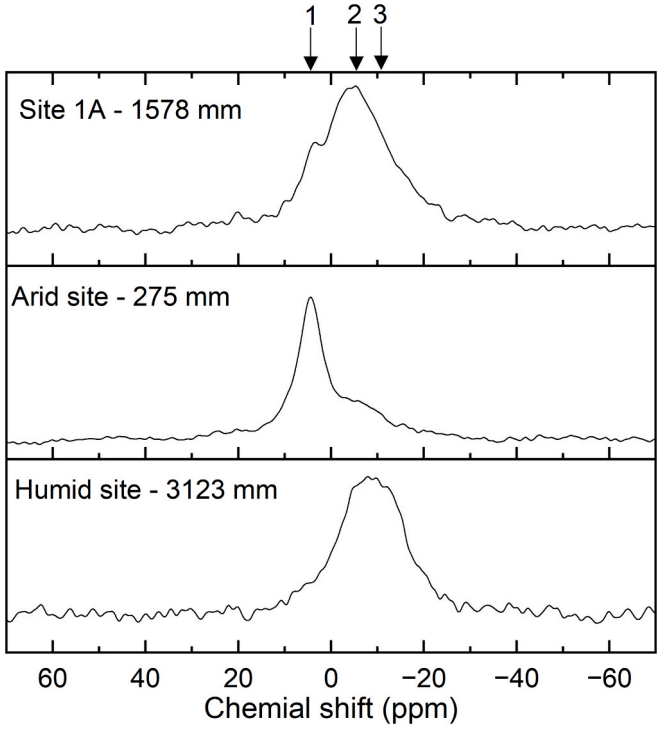

Fig. 6. Solid-state MAS ^{31}P NMR of the A horizon of soils from the three soil process domains (arid – middle; subhumid (Site 1A) – top and humid – bottom) of the Kohala climosequence, Hawaii with mean annual precipitation (in mm y^{-1}); The arrows show the position of 1) apatite, 2) crandallite and 3) wavellite; Reference spectra are shown by Young et al. (2019).

relative to the sensitivity of the technique (Bleam et al., 1989; McDowell et al., 2002). Thus, this is one of the few studies in which we could successfully apply solid state ^{31}P NMR on soils. The NMR results confirm the presence of crandallite in the bulk soil of site 1A and suggest that this mineral was not strongly crystallized. The NMR results are also coherent with the current knowledge on apatite weathering in Al-rich tropical systems. In these systems, P in apatite observed here in the drier site is yields first millisite (not observed here), then crandallite, and then wavellite which is probably present in the wetter site (Borggaard et al., 2012; Hewawasam, 2013; Tercinier, 1972; Vieillard et al., 1979).

Recent years have given rise to analytical methods that have enabled new perspectives on soil phosphorus (Kizewski et al., 2011; Kruse et al., 2015; van der Bom et al., 2022; Vogel et al., 2016). Rather than inferring soil P speciation and sorption processes from bulk chemical data and XRD patterns, methods such as micro-XANES and infrared spectroscopy have enabled more precise detection of P forms at the microscale, as well as their spatial distribution. Bulk FT-IR spectroscopy was already successfully applied for fertilizer/soil mixtures, but in the past only with amounts of P fertilizers added to soils that were well above realistic application rates (Beaton et al., 1963). However, using micro-focused FT-IR spectroscopy, the detection limits can be significantly decreased in comparison to bulk IR spectroscopy (Vogel et al., 2013; Vogel et al., 2016), because during mapping areas of concentrated P at the micrometer scale can be analyzed (Martin et al., 2010). However, no quantification of the share of P species relative to total P can be carried out with this approach because individual measurements are not representative. For IR spectroscopy, reference spectra of crandallite were previously published. Micro-FT-IR spectroscopy corroborated the presence of crandallite at site 2A, circumventing the limitations inherent in bulk FT-IR spectroscopic analytical techniques. However, we detected also several spectra that are close to our crandallite reference, these are probably a mixed mineral with other Al-phosphates. The literature (Breitinger et al., 2006; Frost et al., 2011; Grey et al., 2011) shows that, depending on the sampling spot, the crandallite references have shifts in their bands, because of lattice defects and foreign atoms the lattice.

Phosphorus *K*-edge XANES spectroscopy is increasingly used to elucidate soil P biogeochemistry, and to augment information provided by a suite of complementary methods (e.g., Giguet-Covex et al., 2013; Gu et al., 2020; Helfenstein et al., 2018; Prietzel et al., 2013; Prietzel et al., 2016; Vogel et al., 2021). Evaluation of XANES data with linear combination fitting (Calvin and Furst, 2013; Gustafsson et al., 2020) can determine the major P associations in the soil, if appropriate P reference spectra are used (Eriksson et al., 2016; Werner and Prietzel, 2015). Moreover, the combination of micro-focused X-ray fluorescence (XRF) spectrometry to determine co-localization of P with other elements, and micro-focused XANES spectroscopy can identify P-bearing species present in a heterogeneous sample, including minor species that might not be apparent in bulk spectra (Adediran et al., 2020; Rivard et al., 2016; Vogel et al., 2016). Since no crandallite reference spectra were available from the literature for P *K*-edge XANES, we obtained samples of crandallite and compared the spectra of the mineral sample to soil spectra. Micro-XRF mapping and micro-XANES analysis of site 2 showed that crandallite occurred widely in this soil, in both areas of high P concentration, and in areas of lower P concentration. Furthermore, deviations from the reference spectra suggest that the soils likely contained different variants of Ca-Al-phosphates and not only crandallite in its pure form. The provided spectra can be used by future studies to test for the presence of crandallite in environmental samples.

5. Conclusions

Soil P speciation methods based on “fingerprinting” analyses are only as powerful as the set of P references available for consideration. Due to the fact that crandallite has previously not been considered a major soil P mineral, it has not been used as a reference spectrum in various analysis techniques. Hence, crandallite might have remained undetected in soil P analyses with P *K*-edge XANES, FT-IR, and solid-state NMR spectroscopy. Our approach of coupling various bulk- and micro-spectroscopic techniques for soil P characterization led to the identification of crandallite as an important soil P mineral in the subhumid soils of the Hawaiian climate gradient. Crandallite formation requires available Ca, Al and P, conditions which are favored by neutral to moderately acidic conditions in soils that are not too strongly weathered. In addition, liming and P fertilizer application, which are widespread in agricultural soils, could also create conditions favorable to crandallite formation even in soils which would otherwise not be favorable for crandallite. Including crandallite reference spectra in future

spectroscopic studies is likely to lead to the detection and quantification of more crandallite in soils. Evaluating the global significance of this P mineral will only be possible after more studies consider the potential occurrence of crandallite in soil, and attempt to quantify its prevalence.

CRediT authorship contribution statement

Christian Vogel: Writing – original draft, Visualization, Investigation, Formal analysis, Conceptualization. **Julian Helfenstein:** Writing – original draft, Validation, Methodology, Formal analysis, Conceptualization. **Michael Massey:** Writing – original draft, Methodology, Formal analysis, Conceptualization. **Ruben Kretzschmar:** Writing – review & editing, Investigation, Formal analysis. **Ulrich Schade:** Writing – review & editing, Investigation. **René Verel:** Writing – review & editing, Investigation. **Oliver Chadwick:** Writing – review & editing, Validation, Supervision. **Emmanuel Frossard:** Writing – original draft, Supervision, Resources, Investigation, Funding acquisition, Conceptualization.

Declaration of competing interest

The authors declare that they have no known competing financial interests or personal relationships that could have appeared to influence the work reported in this paper.

Acknowledgments

The CLIMP project (Forms and dynamics of soil phosphorus along a climosequence on basalt-derived soils) was funded by the Swiss National Science Foundation (Project number 200021_162422). CV thanks the German Research Foundation (VO 1794/4-1) for support. Use of the Stanford Synchrotron Radiation Lightsource, SLAC National Accelerator Laboratory, is supported by the U.S. Department of Energy, Office of Science, Office of Basic Energy Sciences under Contract No. DE-AC02-76SF00515. The authors would like to thank Juan S. Lezama-Pacheco for assistance in crandallite XRD data collection, and to gratefully acknowledge the use of the Stanford Environmental Measurement Facility (X-ray Sciences). We thank Charline Giguet-Covex for sharing the Al-humic P reference spectra. Infrared microspectroscopy was conducted on the IRIS beamline at the synchrotron BESSYII from Helmholtz-Zentrum Berlin (HZB). We thank the HZB for allocation of synchrotron radiation beamtime.

Appendix A. Supplementary data

Supplementary data to this article can be found online at https://doi.org/10.1016/j.geoderma.2026.117712.

Data availability

Data will be made available on request.

References

Adams, J.A., Howarth, D.T., Campbell, A.S., 1973. Plumbogummite minerals in a strongly weathered New Zealand soil. J. Soil Sci. 24 (2), 224–231.
Adediran, G.A., Tuyishime, J.R.M., Vantelon, D., Klysubun, W., Gustafsson, J.P., 2020. Phosphorus in 2D: Spatially resolved P speciation in two swedish forest soils as influenced by apatite weathering and podzolization. Geoderma 376, 114550.
Batista, A.H., Melo, V.F., Gilkes, R., 2017. Scanning and transmission analytical electron microscopy (STEM-EDX) identifies minor minerals and the location of minor elements in the clay fraction of soils. Appl. Clay Sci. 135, 447–456.
Beaton, J.D., Charlton, T.L., Speer, R., 1963. Identification of Soil-fertilizer Reaction Products in a Calcareous Saskatchewan Soil by Infra-red Absorption Analysis. Nature 197 (4874), 1329–1330.
Beauchemin, S., Hesterberg, D., Chou, J., Beauchemin, M., Simard, R.R., Sayers, D.E., 2003. Speciation of Phosphorus in Phosphorus-Enriched Agricultural Soils using X-Ray Absorption Near-Edge Structure Spectroscopy and Chemical Fractionation. J. Environ. Qual. 32 (5), 1809–1819.
Bleam, W.F., Pfeffer, P.E., Frye, J.S., 1989. 31P solid-state nuclear magnetic resonance spectroscopy of aluminum phosphate minerals. Phys. Chem. Miner. 16 (5), 455–464.
Bolland, M.D.A., Allen, D.G., 1987. Comparison of three soil tests for phosphate on lateritic soil fertilized with superphosphate, crandallite rock phosphates and apatite rock phosphates. Soil Res. 25 (4), 555–562.
Bolland, M.D.A., Gilkes, R.J., 1990. Cultivation reduces fertilizer residual effectiveness and affects soil testing for available phosphorus. Fertilizer Research 24 (1), 33–46.
Borggaard, O.K., Koch, C.B., Elberling, B., Breuning-Madsen, H., Stemmerik, L., 2012. Composition of characteristic soils on the raised atoll Bellona, Solomon Islands. Geoderma 170, 186–194.
Breitinger, D.K., Brehm, G., Mohr, J., Colognesi, D., Parker, S.F., Stolle, A., Pimpl, T.H., Schwab, R.G., 2006. Vibrational spectra of synthetic crandallite-type minerals—optical and inelastic neutron scattering spectra. J. Raman Spectrosc. 37 (1–3), 208–216.
Bullen, T., Chadwick, O., 2016. Ca, Sr and Ba stable isotopes reveal the fate of soil nutrients along a tropical climosequence in Hawaii. Chem. Geol. 422, 25–45.
Calvin, S., Furst, K.E., 2013. XAFS for everyone. Crc Press Inc.
Chadwick, O.A., Chorover, J., Chadwick, K.D., Bateman, J.B., Slessarev, E.W., Kramer, M., Thompson, A., Vitousek, P.M., 2022. Constraints of climate and Age on Soil Development in Hawai'i. In: Wymore, A.S., Yang, W.H., Silver, W.L., McDowell, W.H., Chorover, J. (Eds.), Biogeochemistry of the Critical Zone. Springer International Publishing, Cham, pp. 49–88.
Chadwick, O.A., Gavenda, R.T., Kelly, E.F., Ziegler, K., Olson, C.G., Elliott, W.C., Hendricks, D.M., 2003. The impact of climate on the biogeochemical functioning of volcanic soils. Chem. Geol. 202 (3), 195–223.
Chadwick, O.A., Kelly, E.F., Hotchkiss, S.C., Vitousek, P.M., 2007. Precontact vegetation and soil nutrient status in the shadow of Kohala Volcano. Hawaii. Geomorphology 89 (1), 70–83.
Costa, M., Kern, D., Pinto, A., Souza, J., 2004. The ceramic artifacts in archaeological black earth (terra preta) from lower Amazon Region, Brazil: chemistry and geochemical evolution. Acta Amazon. 34, 375–386.
Doak, B.W., Gallagher, P.J., Evans, L., Muller, F.B., 1965. Low-temperature calcination of "C"-grade phosphate from christmas island. N. Z. J. Agric. Res. 8 (1), 15–29.
Energie, H.Z., 2016. The IRIS THz/Infrared beamline at BESSY II. J. Large-Scale Res. Facilites 2, A95. https://doi.org/10.17815/jlsrf-2-95.
Eriksson, A.K., Hillier, S., Hesterberg, D., Klysubun, W., Ulén, B., Gustafsson, J.P., 2016. Evolution of phosphorus speciation with depth in an agricultural soil profile. Geoderma 280, 29–37.
Farmer, V.C., 1974. The Infrared Spectra of Minerals. Mineralogical Society, London.
Fieldes, M., Bealing, G., Claridge, G.G., Wells, N., Taylor, N.H., 1960. Mineralogy and radioactivity of Niue Island soils. N. Z. J. Sci. 3, 658–675.
Fischer, P., Pöthig, R., Gücker, B., Venohr, M., 2018. Phosphorus saturation and superficial fertilizer application as key parameters to assess the risk of diffuse phosphorus losses from agricultural soils in Brazil. Sci. Total Environ. 630, 1515–1527.
Francisco, E.A.B., Prochnow, L.I., Motta de Toledo, M.C., Pereira, J.P., 2008. Agronomic Evaluation of Calcined Crandallite from three Brazilian Phosphate Deposits. Commun. Soil Sci. Plant Anal. 39 (3–4), 559–573.
Frossard, E., Brossard, M., Hedley, M.J., Metherell, A.K., 1995. Reactions controlling the cycling of P in soils. In: Tiessen, H. (Ed.), Phosphorus in the Global Environment: Transfers, Cycles and Management. John Wiley, New York, pp. 107–137.
Frossard, E., Condron, L.M., Oberson, A., Sinaj, S., Fardeau, J.C., 2000. Processes Governing Phosphorus Availability in Temperate Soils. J. Environ. Qual. 29 (1), 15–23.
Frost, R.L., Xi, Y., Palmer, S.J., Pogson, R., 2011. Vibrational spectroscopic analysis of the mineral crandallite CaAl3(PO4)2(OH)5·(H2O) from the Jenolan Caves, Australia. Spectrochim. Acta A Mol. Biomol. Spectrosc. 82 (1), 461–466.
Garrett, R.G., Porter, A.R.D., Hunt, P.A., 2010. An occurrence of cadmiferous phosphorite soil concretions in Jamaica. Appl. Geochem. 25 (7), 1047–1055.
Giambelluca, T.W., Chen, Q., Frazier, A.G., Price, J.P., Chen, Y.-L., Chu, P.-S., Eischeid, J. K., Delparte, D.M., 2013. Online Rainfall Atlas of Hawai'i. Bull. Am. Meteorol. Soc. 94 (3), 313–316.
Giguet-Covex, C., Poulenard, J., Chalmin, E., Arnaud, F., Rivard, C., Jenny, J.P., Dorioz, J.M., 2013. XANES spectroscopy as a tool to trace phosphorus transformation during soil genesis and mountain ecosystem development from lake sediments. Geochim. Cosmochim. Acta 118, 129–147.
Goldberg, P., Nathan, Y., 1975. The Phosphate Mineralogy of et-Tabun Cave, Mount Carmel, Israel. Mineral. Mag. 40, 253–258.
Grey, I.E., Shanks, F.L., Wilson, N.C., Mumme, W.G., Birch, W.D., 2011. Carbon incorporation in plumbogummite-group minerals. Mineral. Mag. 75 (1), 145–158.
Gu, C., Dam, T., Hart, S.C., Turner, B.L., Chadwick, O.A., Berhe, A.A., Hu, Y., Zhu, M., 2020. Quantifying Uncertainties in Sequential Chemical Extraction of Soil Phosphorus using XANES Spectroscopy. Environ. Sci. Technol. 54 (4), 2257–2267.
Gu, C., Margenot, A.J., 2021. Navigating limitations and opportunities of soil phosphorus fractionation. Plant and Soil 459 (1), 13–17.
Gustafsson, J.P., Braun, S., Tuyishime, J.R.M., Adediran, G.A., Warrinnier, R., Hesterberg, D., 2020. A Probabilistic Approach to Phosphorus Speciation of Soils Using P K-edge XANES Spectroscopy with Linear Combination Fitting. Soil Sys. 4 (2), 26.
Hedley, M.J., Stewart, J.W.B., Chauhan, B.S., 1982. Changes in Inorganic and Organic Soil Phosphorus Fractions Induced by Cultivation Practices and by Laboratory Incubations. Soil Sci. Soc. Am. J. 46 (5), 970–976.
Helfenstein, J., Frossard, E., Pistocchi, C., Chadwick, O., Vitousek, P., Tamburini, F., 2021. Soil Phosphorus Exchange as Affected by Drying-Rewetting of three Soils from a hawaiian Climatic Gradient. Frontiers in Soil Science 1.
Helfenstein, J., Ringeval, B., Tamburini, F., Mulder, V.L., Goll, D.S., He, X., Alblas, E., Wang, Y., Mollier, A., Frossard, E., 2024. Understanding soil phosphorus cycling for sustainable development: a review. One Earth 7 (10), 1727–1740.

Helfenstein, J., Tamburini, F., von Sperber, C., Massey, M.S., Pistocchi, C., Chadwick, O. A., Vitousek, P.M., Kretzschmar, R., Frossard, E., 2018. Combining spectroscopic and isotopic techniques gives a dynamic view of phosphorus cycling in soil. Nat. Commun. 9 (1), 3226.
Hewawasam, T., 2013. Behaviour of major elements and mineralogical changes under tropical weathering in two apatite-bearing parent rocks of Sri Lanka. Journal of Geological Society of Sri Lanka 15, 33–49.
Hsieh, J.C.C., Chadwick, O.A., Kelly, E.F., Savin, S.M., 1998. Oxygen isotopic composition of soil water: Quantifying evaporation and transpiration. Geoderma 82 (1), 269–293.
Ingall, E.D., Brandes, J.A., Diaz, J.M., de Jonge, M.D., Paterson, D., McNulty, I., Elliott, W.C., Northrup, P., 2011. Phosphorus K-edge XANES spectroscopy of mineral standards. J. Synchrotron Radiat. 18 (2), 189–197.
Kizewski, F., Liu, Y.-T., Morris, A., Hesterberg, D., 2011. Spectroscopic Approaches for Phosphorus Speciation in Soils and Other Environmental Systems. J. Environ. Qual. 40 (3), 751–766.
Klotzbücher, A., Kaiser, K., Klotzbücher, T., Wolff, M., Mikutta, R., 2019. Testing mechanisms underlying the Hedley sequential phosphorus extraction of soils. J. Plant Nutr. Soil Sci. 182 (4), 570–577.
Koch, M., Kruse, J., Eichler-Löbermann, B., Zimmer, D., Willbold, S., Leinweber, P., Siebers, N., 2018. Phosphorus stocks and speciation in soil profiles of a long-term fertilizer experiment: evidence from sequential fractionation, P K-edge XANES, and 31P NMR spectroscopy. Geoderma 316, 115–126.
Kruse, J., Abraham, M., Amelung, W., Baum, C., Bol, R., Kühn, O., Lewandowski, H., Niederberger, J., Oelmann, Y., Rüger, C., Santner, J., Siebers, M., Siebers, N., Spohn, M., Vestergren, J., Vogts, A., Leinweber, P., 2015. Innovative methods in soil phosphorus research: a review. J. Plant Nutr. Soil Sci. 178 (1), 43–88.
Martin, M.C., Schade, U., Lerch, P., Dumas, P., 2010. Recent applications and current trends in analytical chemistry using synchrotron-based Fourier-transform infrared microspectroscopy. TrAC Trends Anal. Chem. 29 (6), 453–463.
Massey, M.S., 2019. X-Ray Spectroscopic Quantification of Struvite and Dittmarite Recovered from Wastewater. J. Environ. Qual. 48 (1), 193–198.
Massey, M.S., Zohar, I., Ippolito, J.A., Litaor, M.I., 2018. Phosphorus Sorption to Aluminum-based Water Treatment Residuals Reacted with Dairy Wastewater: 2. X-Ray Absorption Spectroscopy. J. Environ. Qual. 47 (3), 546–553.
McDowell, R.W., Brookes, P.C., Mahieu, N., Poulton, P.R., Johnston, A.E., Sharpley, A.N., 2002. The effect of soil acidity on potentially mobile phosphorus in a grassland soil. J. Agric. Sci. 139 (1), 27–36.
Nriagu, J.O., 1976. Phosphate – clay mineral relations in soils and sediments. Can. J. Earth Sci. 13 (6), 717–736.
Nriagu, J.O., 1984. Phosphate Minerals: their Properties and General Modes of Occurrence. In: Nriagu, J.O., Moore, P.B. (Eds.), Phosphate Minerals. Springer, Berlin Heidelberg, Berlin, Heidelberg, pp. 1–136.
Porder, S., Chadwick, O.A., 2009. Climate and soil-age constraints on nutrient uplift and retention by plants. Ecology 90 (3), 623–636.
Prietzel, J., Dümig, A., Wu, Y., Zhou, J., Klysubun, W., 2013. Synchrotron-based P K-edge XANES spectroscopy reveals rapid changes of phosphorus speciation in the topsoil of two glacier foreland chronosequences. Geochim. Cosmochim. Acta 108, 154–171.
Prietzel, J., Klysubun, W., Werner, F., 2016. Speciation of phosphorus in temperate zone forest soils as assessed by combined wet-chemical fractionation and XANES spectroscopy. J. Plant Nutr. Soil Sci. 179 (2), 168–185.
Ravel, B., Newville, M., 2005. ATHENA, ARTEMIS, HEPHAESTUS: data analysis for X-ray absorption spectroscopy using IFEFFIT. J. Synchrotron Radiat. 12 (4), 537–541.
Rivard, C., Lanson, B., Cotte, M., 2016. Phosphorus speciation and micro-scale spatial distribution in North-American temperate agricultural soils from micro X-ray fluorescence and X-ray absorption near-edge spectroscopy. Plant and Soil 401 (1), 7–22.
Siegenthaler, M.B., Tamburini, F., Frossard, E., Chadwick, O., Vitousek, P., Pistocchi, C., Mészáros, É., Helfenstein, J., 2020. A dual isotopic (32P and 18O) incubation study to disentangle mechanisms controlling phosphorus cycling in soils from a climatic gradient (Kohala, Hawaii). Soil Biol. Biochem. 149, 107920.
Spengler, S.R., Garcia, M.O., 1988. Geochemistry of the Hawi lavas, Kohala Volcano, Hawaii. Contrib. Miner. Petrol. 99 (1), 90–104.
Tercinier, G., 1972. La crandallite, phosphate naturel répandu dans les sols et souvent abondant dans les produits de remplissage des karsts. Comptes Rendus De L'académie Des Sciences. Série D : Sciences Naturelles 274 (10), 1445–1448.
van der Bom, F.J.T., Kopittke, P.M., Raymond, N.S., Sekine, R., Lombi, E., Mueller, C.W., Doolette, C.L., 2022. Methods for assessing laterally-resolved distribution, speciation and bioavailability of phosphorus in soils. Reviews in Environmental Science and. Bio/Technology.
Vieillard, P., Tardi, Y., Nahon, N., 1979. Stability fields of clays and aluminum phosphates: paragenesis in lateritic weathering of argillaceous phosphatic sediments. Am. Mineral. 64, 624–634.
Vitousek, P.M., Chadwick, O.A., 2013. Pedogenic Thresholds and Soil Process Domains in Basalt-Derived Soils. Ecosystems 16 (8), 1379–1395.
Vogel, C., Adam, C., Sekine, R., Schiller, T., Lipiec, E., McNaughton, D., 2013. Determination of Phosphorus Fertilizer Soil Reactions by Raman and Synchrotron Infrared Microspectroscopy. Appl. Spectrosc. 67 (10), 1165–1170.
Vogel, C., Helfenstein, J., Massey, M.S., Sekine, R., Kretzschmar, R., Beiping, L., Peter, T., Chadwick, O.A., Tamburini, F., Rivard, C., Herzel, H., Adam, C., Pradas del Real, A. E., Castillo-Michel, H., Zuin, L., Wang, D., Félix, R., Lassalle-Kaiser, B., Frossard, E., 2021. Microspectroscopy reveals dust-derived apatite grains in acidic, highly-weathered hawaiian soils. Geoderma 381, 114681.
Vogel, C., Rivard, C., Tanabe, I., Adam, C., 2016. Microspectroscopy - Promising Techniques to Characterize Phosphorus in Soil. Commun. Soil Sci. Plant Anal. 47 (18), 2088–2102.
Walker, T.W., Syers, J.K., 1976. The fate of phosphorus during pedogenesis. Geoderma 15 (1), 1–19.
Webb, S.M., 2005. SIXpack: a graphical user interface for XAS analysis using IFEFFIT. Phys. Scr. 2005 (T115), 1011.
Werner, F., Prietzel, J., 2015. Standard Protocol and Quality Assessment of Soil Phosphorus Speciation by P K-Edge XANES Spectroscopy. Environ. Sci. Technol. 49 (17), 10521–10528.
Williams, J.D.H., Mayer, T., Nriagu, J.O., 1980. Extractability of Phosphorus from Phosphate Minerals Common in Soils and Sediments. Soil Sci. Soc. Am. J. 44 (3), 462–465.
Young, N.J., Coley, M.D., Greenaway, A.M., 2019. Mineralogical investigations of Jamaican hematite-rich and goethite-rich bauxites using XRD and solid state 27Al and 31P MAS NMR spectroscopy. J. Geochem. Explor. 200, 54–76.